PRP Pharmacology Research & Perspectives
Open Access

ORIGINAL ARTICLE

Functional imaging of pharmacological action of SGLT2 inhibitor ipragliflozin via PET imaging using ^{11}C-MDG

Keisuke Mitsuoka, Yuka Hayashizaki, Yoshihiro Murakami, Toshiyuki Takasu, Masanori Yokono, Nobuhiro Umeda, Shoji Takakura, Akihiro Noda & Sosuke Miyoshi

Drug Discovery Research, Astellas Pharma Inc., Tsukuba, Japan

Keywords
Ipragliflozin and visualization, MDG, PET, SGLT2

Correspondence
Sosuke Miyoshi, Drug Discovery Research, Astellas Pharma Inc., 21 Miyukigaoka, Tsukuba 305-8585 Japan. Tel: +81 29 829 6476; Fax: +81 29 85 1879;
E-mail: sousuke.miyoshi@astellas.com

Funding Information
This study was funded by Astellas Pharma Inc.

Received: 9 December 2015; Revised: 26 May 2016; Accepted: 30 May 2016

Pharma Res Per, 4(4), 2016, e00244, doi:10.1002/prp2.244

doi: 10.1002/prp2.244

This study was presented in part at the 57th JDS Annual Meeting, Osaka, Japan, May 22–24, 2014, Poster #1216; the SNMMI Annual Meeting June 7–11, 2014, St. Louis, Missouri, No. 1216; and the American Diabetes Association 74th Scientific Sessions June 13–17, 2014, San Francisco, California, 1037-P.

Recommended section assignment: Drug Discovery and Translational Medicine

Abstract

Sodium-dependent glucose cotransporter 2 (SGLT2) is a pharmacological target of type 2 diabetes mellitus. The aim of this study was to noninvasively visualize the pharmacological action of a selective SGLT2 inhibitor ipragliflozin in the kidney using positron emission tomography (PET) imaging with ^{11}C-methyl-D-glucoside (^{11}C-MDG), an SGLT-specific radio-labeled substrate. PET imaging with ^{11}C-MDG in vehicle-treated rats demonstrated that intravenously injected ^{11}C-MDG substantially accumulated in the renal cortex, reflecting that the compound was reabsorbed by SGLTs. In contrast, ipragliflozin-treated rats showed significantly lower uptake of ^{11}C-MDG in renal cortex in a dose-related manner, suggesting that ipragliflozin inhibited the renal reabsorption of ^{11}C-MDG. This method of visualizing the mode of action of an SGLT2 inhibitor in vivo has demonstrated the drug's mechanism in reducing renal glucose reabsorption in kidney in living animals.

Abbreviations

^{11}C-MDG, ^{11}C -Methyl-D-glucoside; ^{18}F-FDG, ^{18}F-Fluorodeoxyglucose; GLUT, Glucose transporter; MRI, Magnetic resonance imaging; PET, Positron emission tomography; ROI, Region of interest; SGLT, Sodium-dependent glucose cotransporter; T2DM, Type 2 diabetes mellitus.

Introduction

Type 2 diabetes mellitus (T2DM) is a major metabolic disorder afflicting an increasing number of patients around the world. T2DM is characterized by hyperglycemia, in which an excessive amount of glucose circulates in the blood. However, maintaining good glycemic control using conventional antihyperglycemic agents is difficult in most T2DM patients, due to either or both limited efficacy or adverse side effect such as weight gain, hypoglycemia, and gastrointestinal discomfort (Inzucchi 2002).

Recent studies have identified sodium-dependent glucose cotransporter 2 (SGLT2) inhibitors as a new class of drugs useful in treating T2DM (Abdul-Ghani and DeFronzo 2008; Bakris et al. 2009; Faham et al. 2008; Idris and Donnelly 2009; Poudel 2013). SGLT2 is a

glucose transporter situated in the S1 segment of the proximal tubule in the renal cortex and contributes to the reabsorption of glomerular-filtered glucose. Thus, SGLT2 inhibitors induce increased urinary glucose excretion by inhibiting renal glucose reabsorption, exerting a subsequent antihyperglycemic effect. Pharmacological mechanism of SGLT2 inhibitor is well understood as a mechanistic model has been reported to describe its pharmacokinetics–pharmacodynamics behavior of SGLT2 inhibitors (Demin et al. 2014). Although increases in urinary glucose excretion are a known consequence of the pharmacological action of SGLT2 inhibitors, the pharmacological action of these inhibitors at the kidney has not been directly visualized in living animals.

Positron emission tomography (PET) is a molecular imaging methodology that enables visualization of spatial and temporal distribution as well as quantification of radio-labeled molecules of interest. ^{11}C-methyl-D-glucoside (^{11}C-MDG), a metabolically stable positron emitter, is a selective substrate of SGLTs (Bormans et al. 2003). After filtration through renal glomeruli, ^{11}C-MDG is reabsorbed by SGLTs into renal proximal tubular cells in the renal cortex (Fig. 1). Given that ^{11}C-MDG is not a substrate of glucose transporters (GLUTs), it is not transported by GLUT2, which is located in the basolateral membrane, leaving ^{11}C-MDG to instead accumulate in cells in the renal cortex (Bormans et al. 2003). PET imaging using ^{11}C-MDG is therefore considered appropriate for application in visualizing SGLT function in the kidney.

Ipragliflozin is one SGLT2 inhibitor which has been shown to induce an increase in urinary glucose excretion as well as reduce plasma glucose levels and decrease body weight in clinical studies (Fonseca et al. 2013; Wilding et al. 2013; Kashiwagi et al. 2014; Poole and Dungo 2014). Here, we utilized noninvasive PET imaging to directly observe how an SGLT2 inhibitor affects renal glucose reabsorption in living animals.

Materials and Methods

Drugs

Ipragliflozin L-proline was synthesized at Astellas Pharma Inc. (Ibaraki, Japan). The compound was suspended in 0.5% methylcellulose solution for oral administration and given at 5 mL/kg of body weight. The vehicle treatment group received 0.5% methylcellulose solution. All dosage levels of ipragliflozin in this report are expressed as proline-free substance.

Animals

Male Crj: CD (SD) rats, aged 5–7 weeks, were housed at Tsukuba Research Center of Astellas Pharma Inc. (Ibaraki, Japan) for urinary glucose excretion measurement, Shin Nippon Biochemical Laboratories, Ltd. (SNBL; Tokyo, Japan), for plasma concentration measurement, and Molecular Imaging, Inc. (Ann Arbor, MI, USA) for imaging analysis. All animal experimental procedures were approved by the Institutional Animal Care and Use Committee of Tsukuba Research Center of Astellas Pharma Inc. and Molecular Imaging, Inc., which are accredited by the Association for Assessment and Accreditation of Laboratory Animal Care international (AAALAC international).

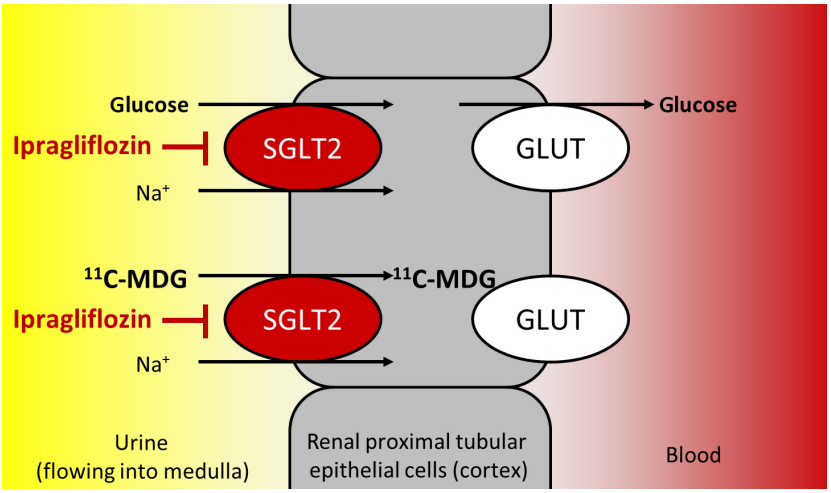

Figure 1. Schematic concept of PET imaging using SGLT-specific substrate ^{11}C-MDG. Ipragliflozin inhibits uptake of ^{11}C-MDG into renal proximal tubular epithelial cells, located in renal cortex, via SGLT2. PET, Positron emission tomography.

Urinary glucose excretion

At 7 weeks of age, rats were allocated to five groups of five animals each, such that each group had similar mean body weights. Rats were orally given vehicle or ipragliflozin (0.3, 1, 3, 10 mg/kg) and then placed into metabolic cages individually. Spontaneously voided urine was collected for 1 h under free access to water and chow. Urinary glucose levels were measured using Glucose CII-Test reagent (Wako Pure Chemical Industries, Ltd., Osaka, Japan).

Plasma concentration of ipragliflozin

At 7 weeks of age, rats were allocated to four groups of three animals each, such that each group had similar mean body weights. Rats were orally given ipragliflozin (0.3, 1, 3, 10 mg/kg). One hour after ipragliflozin administration, rats were anesthetized with 2% isoflurane, and then blood was collected from the inferior vena cava for plasma ipragliflozin concentration measurement.

PET imaging study

Synthesis of ^{11}C-MDG was carried out as described previously (Bormans et al. 2003). PET scanning was performed using Siemens microPET scanners (Siemens, Munich, Germany) as described previously with some modification (Shirakawa et al. 2013; Kaneko et al. 2014). PET imaging studies were performed in three phases, with four rats allocated to designated groups in each phase and used under nonfasted conditions. Body temperature of each rat was maintained using a thermostat-regulated recirculating water-heated pad throughout the imaging procedures. Individual body weights were recorded before each imaging session.

Phase 1: dynamics of ^{11}C-MDG renal uptake (vehicle vs. ipragliflozin)

Rats were dosed either with vehicle or ipragliflozin (3 mg/kg) 1 h before initiation of a PET dynamic scan. Approximately 10–15 min prior to image acquisition, the rats were anesthetized with 2% isoflurane, and a Teflon catheter was inserted into the tail vein for ^{11}C-MDG administration. At the initiation of a 60-min dynamic emission scan, ^{11}C-MDG was administered (0.84–0.95 mCi) in 500 μL of saline, followed by a 300-μL saline flush.

Phase 2: dose–response of ipragliflozin on ^{11}C-MDG renal uptake

PET static scans were started 1 h after administration of ipragliflozin (0.3, 1, 3, 10 mg/kg). Approximately 20 min prior to the scheduled image acquisition, rats were anesthetized with 2% isoflurane, and a Teflon catheter was inserted into the tail vein for ^{11}C-MDG administration. At 10 min prior to the start of a static scan, ^{11}C-MDG was administered (0.80–1.02 mCi) in 500 μL of saline, followed by a 300-μL saline flush.

Phase 3: duration of renal uptake inhibition by ipragliflozin

PET static scans were started 1, 4, and 8 h after administration of ipragliflozin (3 mg/kg) and 1 h after administration of vehicle. Approximately 20 min prior to the scheduled image acquisition, the rats were anesthetized with 2% isoflurane, and a Teflon catheter was inserted into the tail vein for ^{11}C-MDG administration. At 10 min prior to the start of a static scan, ^{11}C-MDG was administered (0.80–1.02 mCi) in 500 μL of saline, followed by a 300-μL saline flush.

In the ^{18}F-fluorodeoxyglucose (^{18}F-FDG) PET study, synthesis of ^{18}F-FDG was carried out as described previously (Shirakawa et al. 2013; Kaneko et al. 2014). PET images were acquired 10–15 min after ^{18}F-FDG administration with or without administration of 3 mg/kg ipragliflozin 60 min before image acquisition. One rat each was allocated to either the ipragliflozin-treated or vehicle-treated groups and used under nonfasted conditions.

Image analysis

The PET list mode data were converted into two-dimensional (2D) sinograms, corrected for random coincidences, and normalized for scanner uniformity. Dynamic PET images were histogrammed into 5-min frames prior to reconstruction. All dynamic and static data were reconstructed using a three-dimensional ordered subsets expectation-maximization algorithm followed by maximum a posteriori reconstruction. The renal cortex, medulla, and pelvis were manually segmented for each kidney individually in the PET images. Radioactivity in each segment was expressed as a product of mean standard uptake value (SUV) and volume of each segment, with mean radioactivity of both kidneys in each rat. Total radioactivity in whole kidney was calculated as the sum of the radioactivity in the renal cortex, medulla, and pelvis. Magnetic resonance imaging (MRI) was performed using a Varian 7T MRI system (Varian, Palo Alto, CA) to obtain anatomical reference of the abdominal region (Fig. S1) to set spatial ROIs of renal cortex, medulla, and pelvis in each PET image of the rats. A T2-weighted spin-echo sequence was used for imaging of the abdominal region.

Statistical analysis

Experimental results are expressed as mean ± standard error (SE). In urinary glucose excretion experiments, Dunnett's multiple-comparison test was used to analyze differences between the ipragliflozin-treated groups and the vehicle-treated group. In the analysis of PET imaging, Dunnett's multiple-comparison test was used for comparisons among multiple groups. A value of $P < 0.05$ was taken as significant. Statistical and data analyses were conducted using GraphPad Prism software (GraphPad Software, Inc., San Diego, CA).

Results

Plasma concentration of ipragliflozin

Plasma concentrations of ipragliflozin increased proportionally to doses at 0.3, 1, 3, and 10 mg/kg (Fig. 2A). Unbound plasma concentration of ipragliflozin 1 h after 0.3 mg/kg dosing was 3.8 ng/mL, which is comparable to the IC_{50} value of the compound against rat SGLT2 (Tahara et al. 2012).

Urinary glucose excretion

Cumulative urinary glucose excretion was measured 0–1 h after oral administration of 0.3, 1, 3, and 10 mg/kg of ipragliflozin. Ipragliflozin increased urinary glucose excretion in a dose-dependent manner (Fig. 2B), with statistical significance versus vehicle-treated group observed in groups dosed with 1, 3, and 10 mg/kg.

PET imaging

In Phase 1 of the PET imaging study, distributional changes in ^{11}C-MDG in the kidney were acquired with or without ipragliflozin administration (Fig. 3A). In rats dosed with vehicle, transient but marked accumulation of ^{11}C radioactivity in the renal cortex was observed, peaking at 5–10 min after PET scan initiation (Fig. 3B). In contrast, in rats dosed with 3 mg/kg of ipragliflozin 1 h prior to imaging, ^{11}C radioactivity was distributed throughout the kidney and gradually concentrated in the renal medulla (Fig. 3B). ^{11}C radioactivity was higher in the bladders of ipragliflozin-treated rats than in those of vehicle-treated rats (Fig. S2). Notably, PET scans of ^{18}F-FDG showed accumulation of tracer radioactivity in the renal medulla of rats, which was not affected by ipragliflozin administration (Fig. S3).

The time course of ^{11}C-MDG radioactivity in the rat kidney differed between vehicle- and ipragliflozin-treated groups (Fig. 3B and C). The time course of ^{11}C-MDG radioactivity showed that the radioactivity in the renal cortex, which peaked at 5 min after scan initiation, was lower in the ipragliflozin-treated group than that in the vehicle-treated group, whereas the radioactivity in the renal medulla and pelvis, which peaked at 15 min after scan initiation, was higher in the ipragliflozin-treated group over the 60-min scanning period (Fig. 3C). Total radioactivity in the kidney decreased more rapidly in the ipragliflozin-treated group than in the vehicle-treated group (Fig. 3C). The time course of ^{11}C-MDG radioactivity in each region of kidney is visualized in cumulative column representation in Figure S4.

In Phase 2 of the PET imaging study, the inhibitory effects of ipragliflozin at a range of doses on ^{11}C-MDG reabsorption were evaluated. The radioactivity in the renal cortex was suppressed by ipragliflozin administration in a dose-related manner, such that administration of 0.3 mg/kg ipragliflozin suppressed radioactivity by 10%, whereas 1 mg/kg and higher doses suppressed values by 50% (Fig. 4).

In Phase 3 of the PET imaging study, duration of the inhibitory effect of ipragliflozin on ^{11}C-MDG reabsorption was evaluated 1, 4, and 8 h after administration of 3 mg/kg ipragliflozin. Radioactivity in renal cortex was

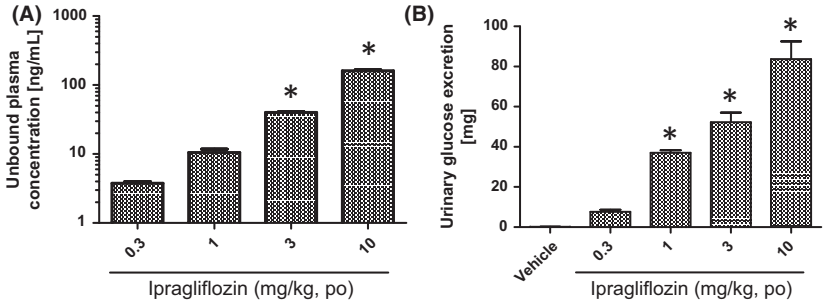

Figure 2. Unbound plasma concentration of ipragliflozin and cumulative urinary glucose excretion in rats. (A) Plasma unbound concentration of ipragliflozin in rats 1 h after oral administration at 0.3, 1, 3, and 10 mg/kg ($n = 3$, mean and SE). (B) Cumulative urinary glucose excretion in rats at 0–1 h after oral administration of ipragliflozin at 0.3, 1, 3, and 10 mg/kg ($n = 5$, mean and SE). *$P < 0.05$ tested by Dunnett's multiple comparison tests.

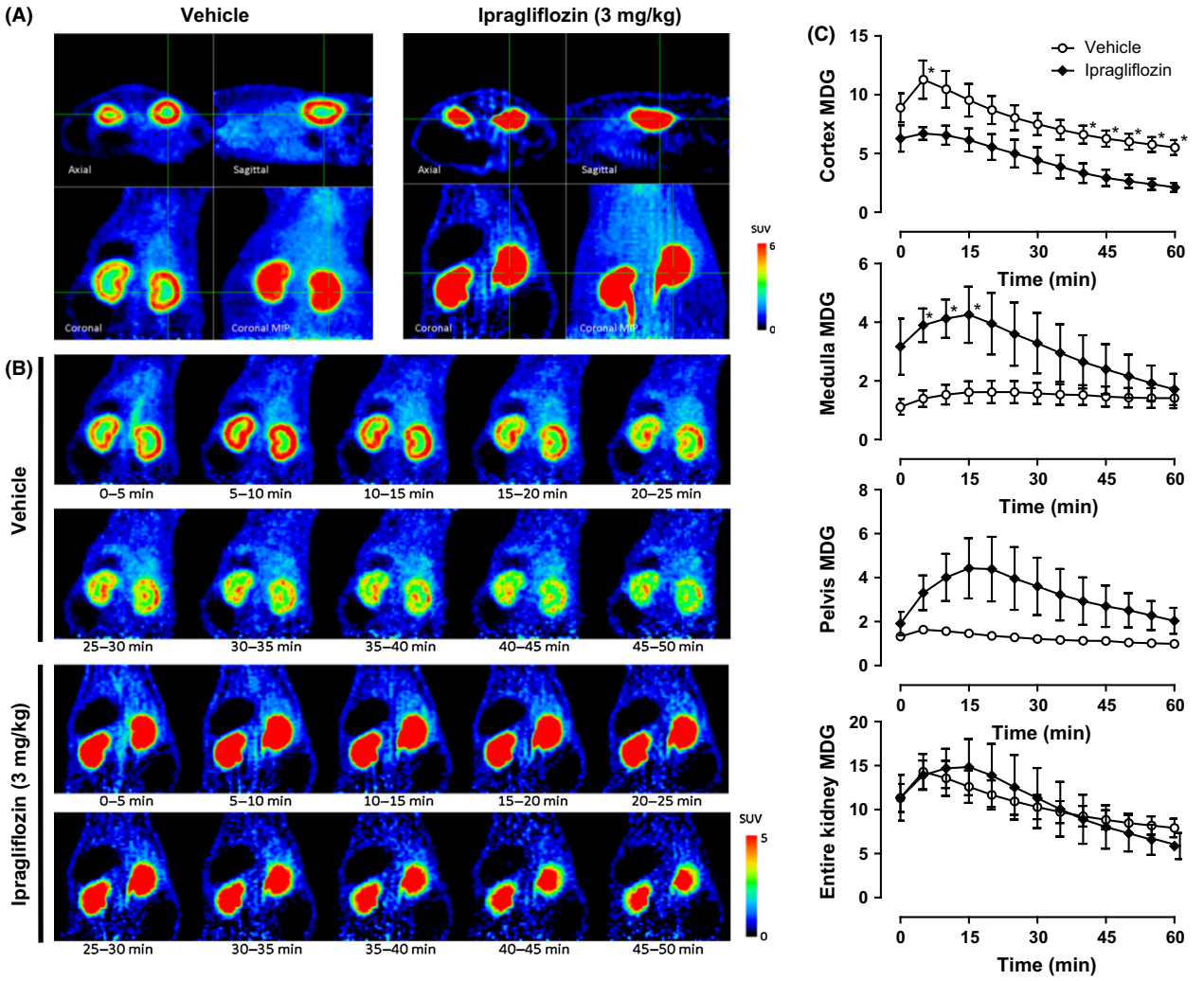

Figure 3. PET images of ^{11}C-MDG in rats dosed with ipragliflozin (3 mg/kg) or vehicle (5 mL/kg). (A) Axial, sagittal, coronal, and coronal MIP images at 5–10-min scan after ^{11}C-MDG administration in each group of rats. Intersection lines are expressed as green lines. (B) Time-lapse PET coronal images of rat kidneys after ^{11}C-MDG intravenous administration with preadministration of vehicle 5 mL/kg 1 h before ^{11}C-MDG dosage, and with preadministration of ipragliflozin 3 mg/kg 1 h before ^{11}C-MDG dosage. (C) Time course of radioactivity changes in renal cortex, medulla, and pelvis as well as whole kidney in vehicle- or ipragliflozin-treated rats (n = 4, mean and SE). The radioactivity in whole kidney is the sum of those in renal cortex, medulla, and pelvis. *P < 0.05 tested by two-tailed Student t-tests. MIP, maximum intensity projection; PET, Positron emission tomography.

significantly lower at all time points after ipragliflozin administration than with vehicle treatment, with maximum suppression at 4 h postadministration (Fig. 5).

Discussion

This study is the first PET imaging study to visualize SGLT function dynamically using SGLT-specific radio-labeled substrate ^{11}C-MDG in living animals. The study also clearly demonstrated the inhibitory effect of ipragliflozin on renal glucose uptake by SGLT2, which had not been directly visualized in vivo.

In previous pharmacology studies using diabetic rats, repeated administration of ipragliflozin decreased HbA1c levels at daily doses ranged from 0.3 mg/kg to 10 mg/kg (Tahara et al. 2012, 2014; Takakura et al. 2016). However, in this study, both plasma concentration of ipragliflozin and enhanced urinary glucose excretion following single oral administration of ipragliflozin were determined. As expected, significant increases in urinary glucose excretion were observed over the initial hour following 1, 3, or 10 mg/kg oral administration of ipragliflozin (Fig. 2B). The unbound fraction of plasma ipragliflozin concentration 1 h after 0.3 mg/kg administration (3.8 ng/mL) was

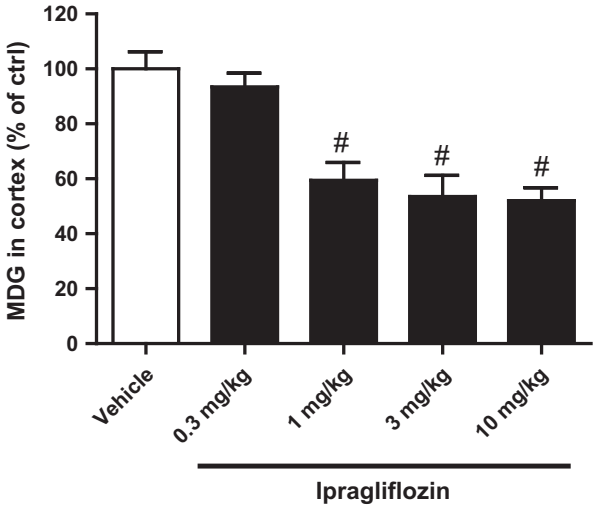

Figure 4. Inhibitory effect of various dose of ipragliflozin on ^{11}C-MDG uptake. MDG radioactivity in renal cortex at 1 h after administration of ipragliflozin (0, 0.3, 1, 3, and 10 mg/kg) is normalized by that in the vehicle-treated group (n = 4, mean and SE). $^{\#}P < 0.05$ tested by Dunnett's multiple comparison tests.

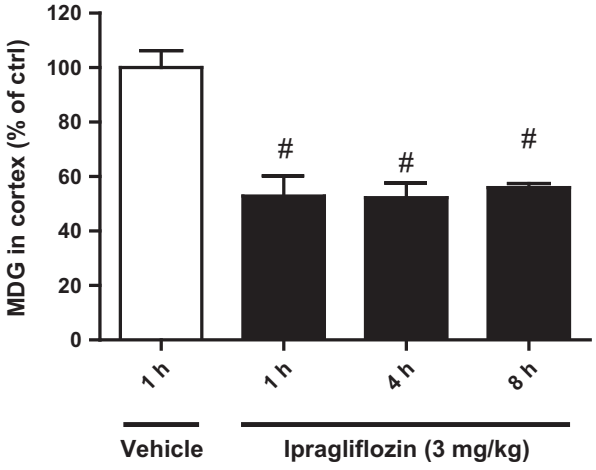

Figure 5. Duration of inhibitory effect of ipragliflozin on renal glucose reabsorption. MDG in cortex indicates ^{11}C-MDG radioactivity in the renal cortex 1 h after administration of vehicle and 1, 4, and 8 h after administration of ipragliflozin (3 mg/kg, n = 4, mean and SE). $^{\#}P < 0.05$ tested by Dunnett's multiple comparison test.

comparable to the IC_{50} value of ipragliflozin against rat SGLT2 (2.72 ng/mL) (Tahara et al. 2012). Based on the concentration inhibition curve of ipragliflozin for rat SGLT2, the plasma concentration of ipragliflozin 1 h after an oral dose of 3 mg/kg (31.9 ng/mL) was estimated to inhibit rat SGLT2 by approximately 90% (Tahara et al. 2012). We therefore used 3 mg/kg of ipragliflozin in subsequent PET imaging studies conducted at 1 or more hours after oral administration of ipragliflozin.

PET imaging with ^{11}C-MDG was applied to visualize the inhibitory effect of ipragliflozin on glucose uptake in kidney by SGLTs. After being filtered through renal glomeruli, ^{11}C-MDG is reabsorbed by SGLTs into renal proximal tubular cells located in the renal cortex (Fig. 1). When SGLTs are inhibited, ^{11}C-MDG passes through the renal tubules into the urine in the renal medulla (Fig. 1). Therefore, accumulation of ^{11}C radioactivity in the renal cortex is considered to be caused by cellular uptake of ^{11}C-MDG by SGLTs. In contrast, the accumulation of ^{11}C radioactivity in the renal medulla and the apparent decrease in the renal cortex after the administration of ipragliflozin are considered to be consequences of inhibition of SGLTs (Fig. 3A). In addition, PET images of ^{11}C-MDG in the bladder clearly demonstrate that ipragliflozin increases urinary excretion of ^{11}C-MDG as a consequence of inhibition of renal glucose reabsorption (Fig. S2). The enhancement and delayed peak of radioactivity in the renal medulla and the pelvis in ipragliflozin-treated rats compared to vehicle-treated rats reflected the migration of ^{11}C-MDG into the renal medulla and the pelvis under inhibition of reabsorption through SGLTs (Fig. 3C). The faster decrease in total radioactivity in whole kidney of ipragliflozin-treated rats compared to that of vehicle-treated rats also suggests that the inhibition of SGLTs by ipragliflozin decreases glucose levels in whole kidney as a consequence of enhanced urinary ^{11}C-MDG excretion (Figs. 3C and S2). Furthermore, the suppressed radioactivity in renal cortex at 1, 4, and 8 h after ipragliflozin administration demonstrates that the inhibitory effect at 3 mg/kg dosage on MDG uptake was maintained at least for 8 h (Fig. 5), which can be explained by the half-life of ipragliflozin in rats (3.61 h) (Imamura et al. 2012). Taken together, our results demonstrate that the inhibition of SGLTs by ipragliflozin altered the behavior of ^{11}C-MDG in the kidney, leading to increased urinary glucose excretion. Spatial distribution of ^{18}F-FDG, a GLUT-specific substrate (Yu et al. 2010) in kidney, was not affected by ipragliflozin, which also supports the notion that the dynamics of ^{11}C-MDG in kidneys affected by ipragliflozin were induced by the inhibitory effect on SGLTs (Fig. S3).

We consider the observed inhibition of renal uptake of ^{11}C-MDG to have been caused by the differential inhibitory effect of ipragliflozin on renal SGLTs. In Phase 2 of this PET imaging study, in which the dose–response of ipragliflozin on ^{11}C-MDG renal uptake was investigated, maximum inhibition of ipragliflozin-induced MDG reabsorption plateaued at approximately 50% (Fig. 4). Given the IC_{50} values of ipragliflozin against rat SGLT1 (471.6 ng/mL) and SGLT2 (2.72 ng/mL) and the estimated plasma concentration of ipragliflozin at 1 h after the highest dose of 10 mg/kg (160.5 ng/mL), this compound is considered to weakly inhibit renal SGLT1 and

near completely inhibit SGLT2. The dose–response effect of ipragliflozin on renal MDG reabsorption indicates the induction of a half-maximal effect of ipragliflozin on renal MDG reabsorption at doses in the range 0.3–1 mg/kg. This finding is consistent with our observation that the unbound concentration of ipragliflozin in plasma at 1 h after a dose of 0.3 mg/kg was comparable to the IC_{50} value of the drug (Fig. 4) (Tahara et al. 2012). We therefore consider the inhibitory effect of ipragliflozin on ^{11}C-MDG reabsorption in kidney to be caused by the pharmacological action of the compound on SGLT2. Interindividual difference and circadian patters of renal blood flow and glucose homeostasis are possible error sources of these data.

The retention of approximately 50% of ^{11}C-MDG in the renal cortex with the high doses of ipragliflozin might be due to either or both uptake by SGLT1 in the S3 segment of the proximal tubule located in the outer medulla, or by the partial volume effect of the renal medulla, which increases the apparent radioactivity in the adjacent renal cortex. ^{11}C-MDG in renal cortex tubules not reabsorbed by SGLTs may also have contributed to the residual 50% retention of ^{11}C-MDG in the renal cortex.

In conclusion, we successfully visualized glucose reabsorption in the kidney and its inhibition by the SGLT2 inhibitor ipragliflozin in rats using a PET imaging technique with the SGLT-specific tracer ^{11}C-MDG. This imaging study visualizing the pharmacological action of ipragliflozin directly and dynamically in vivo has demonstrated the proof of mechanism of SGLT2 inhibitors in living animals. Potential differences in MDG reabsorption between normal and diabetic rats need to be examined further. As this method using PET technology can be applied clinically in principle, this could be used as a clinical tool to validate the mode of action of SGLT2 inhibitor in humans.

Acknowledgements

We thank Dr. Patrick McConville and Deanne Lister (Molecular Imaging, Inc.) for conducting animal PET imaging and MRI at Molecular Imaging, and Dr. Peter Scott (University of Michigan) for MDG synthesis. We also thank T. Kimura (Astellas Research Technology, Inc., Ibaraki, Japan) and J. Mizusawa (KAC Co., Ltd., Kyoto, Japan) for assisting with the PET imaging studies at Tsukuba Research Center.

Author Contribution

Participated in research design: K. Mitsuoka, Y. Hayashizaki, Y. Murakami, T. Takasu, M. Yokono, N. Takakura, A. Noda, and S. Miyoshi. Conducted experiments: K. Mitsuoka, Y. Hayashizaki, T. Takasu, and M. Yokono. Performed data analysis: K. Mitsuoka, Y. Hayashizaki, Y. Murakami, T. Takasu, M. Yokono, N. Umeda, S. Takakura, A. Noda, and S. Miyoshi. Wrote or contributed to the writing of the manuscript: K. Mitsuoka, Y. Hayashizaki, T. Takasu, M. Yokono, N. Umeda, S. Takakura, A. Noda, and S. Miyoshi.

Disclosures

All authors are employees of Astellas Pharma Inc. The authors have no further conflicts of interest to disclose.

References

Abdul-Ghani MA, DeFronzo RA (2008). Inhibition of renal glucose reabsorption: a novel strategy for achieving glucose control in type 2 diabetes mellitus. Endocr Pract 14: 782–790.

Bakris GL, Fonseca VA, Sharma K, Wright EM (2009). Renal sodium-glucose transport: role in diabetes mellitus and potential clinical implications. Kidney Int 75: 1272–1277.

Bormans GM, Van Oosterwyck G, De Groot TJ, Veyhl M, Mortelmans L, Verbruggen AM, et al. (2003). Synthesis and biologic evaluation of (11)c-methyl-d-glucoside, a tracer of the sodium-dependent glucose transporters. J Nucl Med 44: 1075–1081.

Demin OJ, Yakovleva T, Kolobkov D, Demin O (2014). Analysis of the efficacy of SGLT2 inhibitors using semi-mechanistic model. Front Phamacol 5: 218.

Faham S, Watanabe A, Besserer GM, Casico D, Specht A, Hirayama BA, et al. (2008). The crystal structure of a sodium galactose transporter reveals mechanistic insights into Na+/sugar symport. Science 321: 810–814.

Fonseca VA, Ferrannini E, Wilding JP, Wilpshaar W, Dhanjal P, Ball G, et al. (2013). Active- and placebo-controlled dose-finding study to assess the efficacy, safety, and tolerability of multiple doses of ipragliflozin in patients with type 2 diabetes mellitus. J Diabetes Complications 27: 268–273.

Idris I, Donnelly R (2009). Sodium-glucose co-transporter-2 inhibitors: an emerging new class of oral antidiabetic drug. Diabetes Obes Metab 11: 79–88.

Imamura M, Nakanishi K, Suzuki T, Ikegai K, Shiraki R, Ogiyama T, et al. (2012). Discovery of Ipragliflozin (ASP1941): a novel C-glucoside with benzothiophene structure as a potent and selective sodium glucose co-transporter 2 (SGLT2) inhibitor for the treatment of type 2 diabetes mellitus. Bioorg Med Chem 20: 3263–3279.

Inzucchi SE (2002). Oral antihyperglycemic therapy for type 2 diabetes: scientific review. JAMA 287:360–372.

Kaneko N, Mitsuoka K, Amino N, Yamanaka K, Kita A, Mori M, et al. (2014). Combination of YM155, a survivin suppressant, with bendamustine and rituximab: a new

combination therapy to treat relapsed/refractory diffuse large B-cell lymphoma. Clin Cancer Res 20: 1814–1822.

Kashiwagi A, Kazuta K, Yoshida S, Nagase I (2014). Randomized, placebo-controlled, double-blind glycemic control trial of novel sodium-dependent glucose cotransporter 2 inhibitor ipragliflozin in Japanese patients with type 2 diabetes mellitus. J Diabetes Investig 5: 382–391.

Poole RM, Dungo RT (2014). Ipragliflozin: first global approval. Drugs 74: 611–617.

Poudel RR (2013). Renal glucose handling in diabetes and sodium glucose cotransporter 2 inhibition. Indian J Endocrinol Metab 17: 588–593.

Shirakawa T, Mitsuoka K, Kuroda K, Miyoshi S, Shiraki K, Naraoka H, et al. (2013). [18F]FDG-PET as an imaging biomarker to NMDA receptor antagonist-induced neurotoxicity. Toxicol Sci 133: 13–21.

Tahara A, Kurosaki E, Yokono M, Yamajuku D, Kihara R, Hayashizaki Y, et al. (2012). Pharmacological profile of ipragliflozin (ASP1941), a novel selective SGLT2 inhibitor, in vitro and in vivo. Naunyn-Schmiedeberg's Arch Pharmacol 385: 423–436.

Tahara A, Kurosaki E, Yokono M, Yamajuku D, Kihara R, Hayashizaki Y, et al. (2014). Effects of sodium-glucose cotransporter 2 selective inhibitor ipragliflozin on hyperglycaemia, oxidative stress, inflammation and liver injury in streptozotocin-induced type 1 diabetic rat. J Pharm Pharmacol 66: 975–987.

Takakura S, Toyoshi T, Hayashizaki Y, Takasu T (2016). Effect of ipragliflozin, an SGLT2 inhibitor, on progression of diabetic microvascular complications in spontaneously diabetic Torii fatty rats. Life Sci 147: 125–131.

Wilding JP, Ferrannini E, Fonseca VA, Wilpshaar W, Dhanjal P, Houzer A (2013). Efficacy and safety of ipragliflozin in patients with type 2 diabetes inadequately controlled on metformin: a dose-finding study. Diabetes Obes Metab 15: 403–409.

Yu AS, Hirayama BA, Timbol G, Liu J, Basarah E, Kepe V, et al. (2010). Functional expression of SGLTs in rat brain. Am J Physiol Cell Physiol 299: C1277–C1284.

Supporting Information

Additional Supporting Information may be found online in the supporting information tab for this article:

Figure S1. Representative coronal display of ^{11}C-MDG PET image co-registered with MRI.
Figure S2. PET images of ^{11}C-MDG in kidney and bladder in rats with or without ipragliflozin administration. The PET images were maximum intensity projection (MIP), axial, sagittal, and coronal images at 4–5 min after administration of saline (5 mL/kg) or ipragliflozin (3 mg/kg). Intersection lines are expressed as green lines.
Figure S3. PET images of ^{18}F-FDG in rat kidneys with or without administration of ipragliflozin (3 mg/kg). The PET images were coronal images at 5 min after administration of saline (5 mL/kg) or ipragliflozin (3 mg/kg).
Figure S4. Accumulative bar graph representing the time course of ^{11}C-MDG activities in the renal cortex, medulla, and pelvis.